Pergamon

PII: S0045-7949(96)00089-2

Computers & Structures Vol. 61, No. 3, pp. 421–430, 1996

0045-7949/96 $15.00 + 0.00

AEROELASTIC ANALYSIS FOR FLAP OF AIRFOIL IN TRANSONIC FLOW

S. Yang and **I. Lee**†

Department of Aerospace Engineering, Korea Advanced Institute of Science and Technology, 373–1, Kusong-dong, Yusong-gu, Taejon, 305–701, Korea

(*Received* 6 *July* 1995)

Abstract—The transonic aeroelastic analyses have been performed for a flap of airfoil. The Euler equations are solved using a finite volume scheme for the aerodynamic calculation. The dynamic grids are generated by a spring analogy method. The unsteady aerodynamic loads are calculated in the time domain and transformed in the frequency domain using a transient pulse technique. The time responses of aeroelastic system are obtained by integrating the structural equations of motion and the unsteady aerodynamic forces using the fourth order Runge–Kutta time stepping method. The aerodynamic loads of airfoils with a flap for the steady and unsteady flow are validated by comparing the present results with the existing experimental data. The aeroelastic time responses for a flapped airfoil are computed for various initial flap angles, structural damping coefficients and Mach numbers. The effects of the stiffness of the flap hinge spring and the initial flap angle on the flutter are also investigated in the transonic speeds. Copyright © 1996 Elsevier Science Ltd.

INTRODUCTION

In the transonic speeds, aerodynamic nonlinearity becomes dominant due to the shock wave or the shock induced separation on the airfoil surface, which result in the most critical flutter problem—the so-called 'transonic dip'. Thus, proper numerical methods are required to obtain accurate transonic aerodynamic loads necessary for the prediction of aeroelastic responses. Many transonic aeroelastic analyses have been performed using the technique of computational fluid dynamics since the mid-1970s. When computers were less developed in the past, the transonic aeroelastic analyses were carried out by the transonic small disturbance or the full potential equations, which require relatively small amounts of computational time. Recently, the Euler and Navier–Stokes equations have been solved for transonic aeroelastic analyses because of the development of high-speed computers [1].

Transonic aeroelastic research studies for two-dimensional airfoils with a trailing edge flap have been performed steadily to study gust alleviation and to help the suppression of flutter problems on fixed wing aircraft. Also, the individual blade control (IBC) technique for trailing edge flaps is used to improve helicopter rotor performances and to reduce rotor blade vibrations. Thus, the aeroelastic studies for helicopter rotors and fixed aircraft wings with auxiliary lift surfaces such as a flap or an aileron has become very popular [2].

In 1976, Magnus and Yoshihara calculated unsteady flows over an oscillating NACA64A006 airfoil with a flap using computational fluid dynamics [3]. Ballhaus and Goorjian also performed unsteady aerodynamic analyses for airfoils with a flap using an economical computational method based on the transonic small disturbance equation [4]. Their calculations were the first attempt to obtain time response analyses of a NACA64A006 airfoil oscillating with pitch degrees of freedom. Yang and Batina [5] and Yang and Chen [6] performed flutter and time response analyses for a NACA64A006 conventional and a MBB A-3 supercritical airfoil oscillating with plunge, pitch, and aileron pitch degrees of freedom using LTRAN2-NLR and USTS programs. Their flutter analyses, carried out in frequency domain and neutral stable conditions, were calculated by time response analyses based on frequency domain results. Steger and Bailey simulated transonic aileron buzz for a NACA651-213 airfoil and compared the results with the experiment [7]. The numerical results in Ref. [7] demonstrated that transonic aileron buzz can be successfully studied using computational fluid dynamics. Chyu and Schiff showed that transonic aileron buzz can be solved effectively using simpler modelling of transonic unsteady aerodynamics [8].

Most of the studies mentioned above relied on simpler methods such as the transonic small disturbance or the full potential equations to analyze transonic unsteady aerodynamic or flutter problems. Some higher level equations were solved on coarse grids so that the results for transonic aeroelastic analyses did not account for the realistic flow features.

† To whom correspondence should be addressed.

In the present paper, aeroelastic analyses are performed for a flap of a two-dimensional airfoil. The steady and unsteady aerodynamic loads are calculated by solving the Euler equations based on a finite volume method. It is assumed in the present analyses that viscous effects are not dominant and the flow separation and/or the vortex bursting phenomena do not occur. The aeroelastic time responses are obtained by solving the coupled flow and structural equations of motion using a simultaneous integration technique. The generalized aerodynamic force (GAF) calculated by a transient pulse technique is compared with the experimental data in the frequency domain. The steady and unsteady flow computations are validated by comparing the present results with the experimental data for both NACA64A010 and NACA64A006 airfoils. The aeroelastic time responses are computed for a NACA64A006 airfoil to observe flutter characteristics of an aeroelastic system caused by Mach number, structural damping coefficient, initial flap angle and the stiffness of flap hinge spring.

GOVERNING AERODYNAMIC EQUATIONS AND NUMERICAL ALGORITHM

In the present study, the flow quantities are obtained from the two-dimensional time-dependent Euler equations. For unsteady aerodynamic or aeroelastic analyses, an arbitrary Lagrangian–Eulerian (ALE) formulation for the Euler equations is used to calculate flow flux in the computational flow field with moving boundaries. The integral form of the Euler equations by ALE formulation can be written as

$$\frac{\mathrm{d}}{\mathrm{d}t}\int_{A(t)} \mathbf{w}\,\mathrm{d}A + \int_{C(t)} (\bar{\mathbf{f}}\,\mathrm{d}y - \bar{\mathbf{g}}\,\mathrm{d}x) = 0, \qquad (1)$$

where the vector of conserved variable $\mathbf{w}$ and the convective fluxes $\bar{\mathbf{f}}$ and $\bar{\mathbf{g}}$ are given by

$$\mathbf{w} = \begin{bmatrix} \rho \\ \rho u \\ \rho v \\ \rho e \end{bmatrix},$$

$$\bar{f} = \begin{bmatrix} \rho(u-\xi) \\ \rho(u-\xi)u + p \\ \rho(u-\xi)v \\ \rho(u-\xi)e + up \end{bmatrix},$$

$$\bar{\mathbf{g}} = \begin{bmatrix} \rho(v-\eta) \\ \rho(v-\eta)u \\ \rho(v-\eta)v + p \\ \rho(v-\eta)e + vp \end{bmatrix}, \qquad (2)$$

where ξ and η are the grid line speeds in the x- and y-direction, respectively. Total energy e and total enthalpy H are given by the equation of state for a perfect gas as follows:

$$e = \frac{p}{(\gamma-1)\rho} + \tfrac{1}{2}(u^2+\eta^2); \quad H = e + \frac{p}{\rho}. \qquad (3)$$

The algorithm to solve eqn (1) uses a finite-volume spatial discretization on a structured grid. Artificial dissipation is added explicitly to prevent oscillations near the shock waves and to damp high-frequency uncoupled error modes [9]. The present algorithm also employs enthalpy damping and local time stepping to accelerate to a steady state. However, these are not used for unsteady aerodynamic and aeroelastic analyses in this paper. With respect to boundary conditions, a characteristic analysis based on Riemann invariants is used to determine the values of flow variables on the outer boundary of the grid and a nonreflecting boundary condition is also applied. A normal momentum method is applied to extrapolate necessary pressure from adjacent cell centers to the airfoil surface boundary. The time integration algorithm used in this analysis is the fourth order multi-stage Runge–Kutta, time-stepping scheme.

GRID GENERATION ALGORITHM

The grid generation program is developed to make a necessary grid system without any restriction on geometric shapes such as initial angle of attack of an airfoil, initial flap angle of a kind of airfoil section. This program is composed of four parts. In the first part, an algebraic grid is generated using a multi-surface technique and near-orthogonal grid construction method [10]. In the second part, an elliptic grid is made by the solution of Poisson's equation to improve grid quality [11]. In the third part, the elliptic grid generated in the second part is changed from the initial symmetric airfoil to the other unsymmetric airfoil using the dynamic mesh algorithm. In the last part, an initial angle of attack of the airfoil and/or an initial flap angle are imported into the airfoil mesh system generated in the third part using the dynamic mesh algorithm. Each grid made in each part can be used to prepare the input grid data of the steady and unsteady Euler codes.

The dynamic mesh algorithm applied in the third and fourth parts above can be used to generate not only an initial grid for the solution of steady aerodynamics, but also intermediate grids for unsteady aerodynamics or aeroelastic calculations. This procedure is completely general so that it can treat realistic airfoil or wing motions. The basic algorithm models the mesh as a spring network where each grid line represents a linear spring [12, 13]. The stiffness of each spring is inversely proportional to a specified power of the length of edge. In this study, the specified power is set equal to one. Then the static equilibrium condition of the spring system, which is changed continuously due to the movement of the

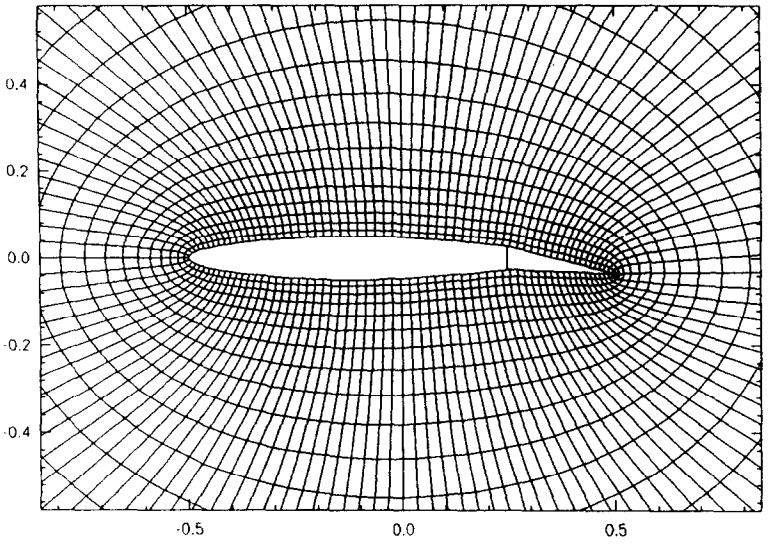

Fig. 1. The O-type grid around the NACA64A010 airfoil with 8° flap angle.

inner boundary computed from the aeroelastic equations of motion at each time step, is solved by a point Jacobi method at each grid point to find a new grid system for the next time step. The grid system generated by this method, which is an O-type and has a NACA64A010 airfoil with 8° flap angle, is shown in Fig. 1.

TRANSIENT PULSE METHOD

To perform the flutter analysis using linear techniques such as p–k or U–g methods, the generalized aerodynamic forces are required for a range of frequencies for each structural vibration mode. The transient pulse method can be effectively used for flutter calculations even for a transonic range, under the assumption that the response for harmonic or aeroelastic motion is a small amplitude of oscillation and the nonlinear characteristics due to shock excursion or viscosity effect is not very large [14]. In the transonic pulse method, a smoothly varying exponentially shaped pulse is used. The input pulse in flap angle is given by

$$\beta(\tau) = \beta_0 + \beta_1 \exp[-(\tau - 17.5\Delta\tau)^2/4], \quad (4)$$

where β_0 is the mean flap angle, β_1 is the amplitude of flap oscillation and $\Delta\tau$ is the nondimensional time step. This method has the advantage that a CFD aerodynamic code is required to be run only once for each Mach number and vibration mode. The procedure is based on the concept of numerical impact simulation. First, an airfoil is forced by the transient exponential pulse given in eqn (4) for an interested structural mode, and then the time history of the resulting flap hinge moment is obtained by solving the unsteady Euler code. The generalized aerodynamic force is obtained in the frequency domain by the fast Fourier transform (FFT) for an input and its response which are calculated through the numerical impact simulation above. In this study, the maximum nondimensional time, $\tau(=U_\infty t/b)$ is set equal to 502.0 for the FFT analysis and the transient response data for 1024 time steps are used.

TIME-MARCHING AEROELASTIC SOLUTIONS

The aeroelastic equation of motion for a flap of an airfoil can be written as

$$[M]\{\ddot{x}\} + [D]\{\dot{x}\} + [K]\{x\} = [B']\{u\}, \quad (5)$$

where

$$[B'] = \frac{U^{*2}}{\pi\mu}\omega_\alpha^2[I]. \quad (6)$$

Here $[M]$, $[D]$, $[K]$, $[B']$ and $[I]$ are mass, damping, stiffness, input and unit matrices, respectively. $\{x\}$ is the perturbation displacement vector and ω_α is the uncoupled frequency of pitch mode, which is set to be 0.826 in the present study. U^* is the nondimensional freestream velocity ($\equiv U_F/(b\omega_\alpha)$), μ is the airfoil mass ratio and $\{u\}$ is the airload vector.

For an airfoil with a flap shown in Fig. 2, the elements of eqn (5) can be given as

$$[M] = r_\beta^2,$$

$$[D] = g_\beta,$$

$$[K] = r_\beta^2\omega_\beta^2,$$

$$\{x\} = (\beta - \beta_0),$$

$$\{u\} = 2(c_n - c_{n0}), \quad (7)$$

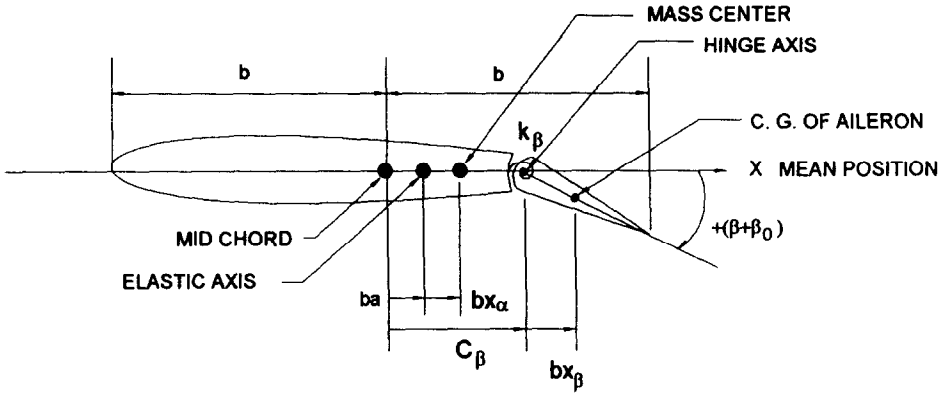

Fig. 2. Parameters and sign convention for an aeroelastic system with a flap.

where r_β is the radius of gyration of flap, g_β is the structural damping coefficient of flap and ω_β is the uncoupled natural frequency of flap about hinge axis. β and β_0 are the total flap and initial flap angles, respectively. c_n and c_{n0} are the total hinge and steady flap moment coefficients, respectively. The hinge moment H, which is positive in the clockwise direction, and c_n are defined as

$$H = q_\infty \oint_{\text{flap}} c_p(x - bc_\beta)c \, dx,$$

$$c_n = H/(q_\infty c^2), \tag{8}$$

where c_p is the pressure coefficient, b is the semi-chord of an airfoil, c is the chord, bc_β is the distance between the mid-chord of the airfoil and the hinge axis and q_∞ is the freestream dynamic pressure.

The state–space form of eqn (5) can be written as

$$\{\dot{y}\} = [A]\{y\} + [B]\{u\}, \tag{9}$$

where

$$\{y\} = \begin{bmatrix} (\beta - \beta_0) \\ (\beta - \beta_0) \end{bmatrix},$$

$$[A] = \begin{bmatrix} 0 & \mathbf{I} \\ -\mathbf{M}^{-1}\mathbf{K} & -\mathbf{M}^{-1}\mathbf{C} \end{bmatrix};$$

$$[B] = \begin{Bmatrix} 0 \\ \mathbf{M}^{-1}\mathbf{B}' \end{Bmatrix}. \tag{10}$$

The solution of eqn (9) is obtained using the subroutine DVERK (IMSL library) based on the 5–6 order Runge–Kutta time integration method. The step-by-step integration procedure for obtaining the aeroelastic response is performed as follows. First, a steady aerodynamic solution is obtained for a given airfoil shape, an initial flap angle and initial freestream conditions. Using the steady flap moment coefficient c_{n0} and initial velocity perturbation β, eqn (9) is solved using the subroutine DVERK, and then the flap displacement, velocity and acceleration are determined at the time step t. The new boundary conditions for the airfoil systems are calculated from the previously determined displacement and velocity, and the intermediate grid system is also determined using the dynamic mesh algorithm at the present time step t. The new aerodynamic forces are computed from the unsteady aerodynamic module in the present aeroelastic computer code. Then all quantities of displacement, velocity and aerodynamic coefficients at the time t are known, so that further computations at the time step $t + \Delta t$ can be carried out. This process is repeated at every time step until the required response is obtained. A flow chart of this procedure is shown in Fig. 3.

RESULTS

Verification of aerodynamic calculation

To validate the accuracy of the present Euler code in the transonic speed, the static results are obtained for a NACA64A010 airfoil with a flap, of which the hinge axis is located at 75% chord station from the leading edge. The grid used in this analysis is a structured O-type grid and the grid size is 129 points in the x = direction and 33 in the y-direction. The far field boundary is located at 20 times the chord length from the airfoil. The flow results are obtained at the free stream Mach number of 0.8 and zero angle of attack of the airfoil. The pressure distributions on the airfoil surface are shown in Fig. 4 and the present results are in a good agreement with the experimental data (0° flap deflection) given in Ref. [15]. When the flap deflection is 2, 4 and 6°, the static pressure results are compared with the Euler results. The shock strength and location are in a good agreement with the results of Ref. [8]. However, the present analysis gives more steep shock waves which are more accurate because the number of grid points used in Ref. [8] [87 points in the $\xi(x)$ direction and 41 points in $\eta(y)$ direction, and 61 points on the airfoil surface] is smaller than that of the present. As the flap deflection increases, the shock wave on the upper surface moves to the trailing edge and the shock strength becomes stronger. On the other hand, the shock wave on the

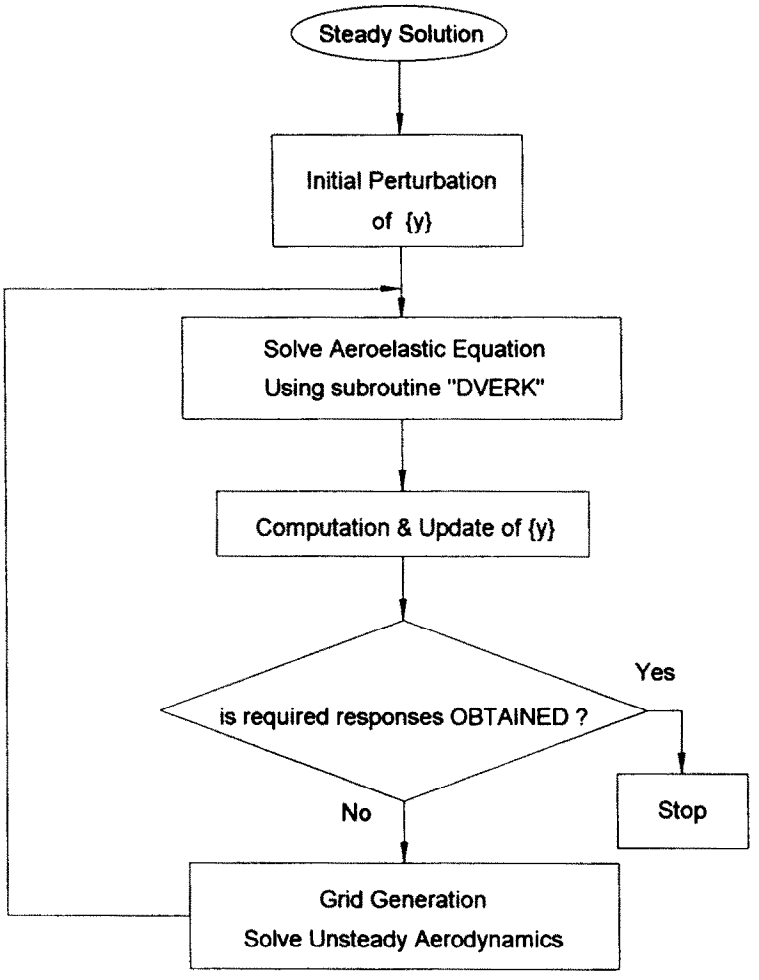

Fig. 3. Flow chart for the analysis of an aeroelastic time response.

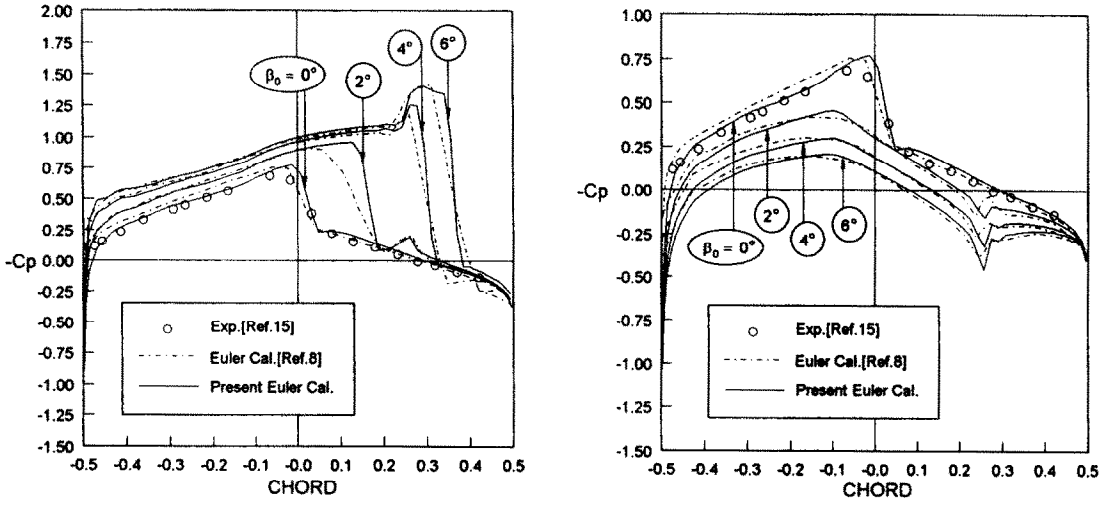

(a) Upper Surface (b) Lower Surface

Fig. 4. Static pressure distributions of the NACA64A010 airfoil at $M_\infty = 0.8$.

lower surface does not appear as the flap deflection increases. From the results mentioned above, it is concluded that the present Euler code gives reasonably accurate solutions.

The unsteady pressure distributions due to the sinusoidal flap motion of an airfoil are obtained to validate the unsteady aerodynamic results of the present Euler code. The grid size is the same as that of the steady case. The results are obtained on the same model as the oscillating flap of Ref. [4] which is a NACA64A006 airfoil with a flap whose flap hinge axis is located at 75% chord from the leading edge. The flap motion is sinusoidal (1° amplitude and 0.179 reduced frequency (k_b) based on the semichord at $M_\infty = 0.854$). The comparisons between the Euler results in Ref. [4] and the present results are shown in Fig. 5. The instantaneous pressure distributions are shown when the flap deflection is 0° ($\omega t = 360°$), +0.866° ($\omega t = 480°$), and −0.866° ($\omega t = 600°$) during the second cycle. Two results are in a good agreement and this agreement was verified at every time step through the second cycle even if the other data are not shown here.

Generalized aerodynamic force

The transient pulse method, which is used to calculate the generalized aerodynamic force (GAF) for flutter analysis, can be used under the flow condition

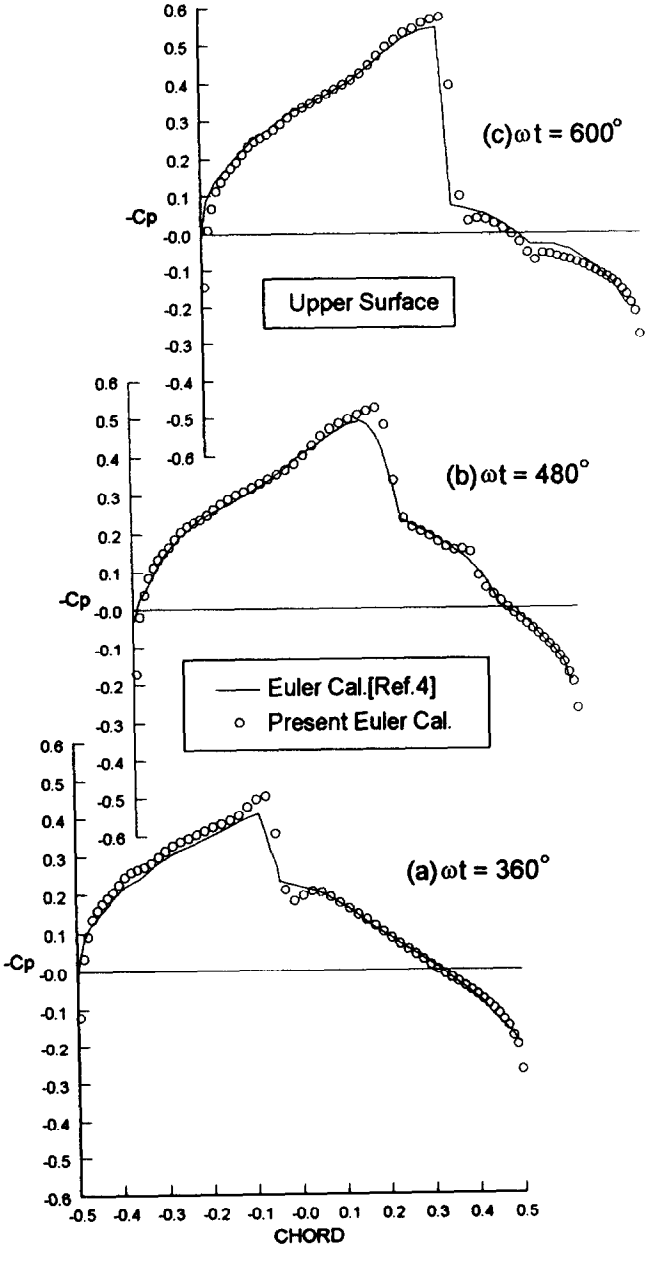

Fig. 5. Instantaneous pressure distributions of the NACA64A006 airfoil with an oscillating trailing edge flap during second cycle ($M_\infty = 0.854$, $k_b = 0.179$).

that the effects of aerodynamic nonlinearities do not appear or are almost neglected. The analysis model is chosen as the NACA64A006 airfoil with a flap, whose hinge axis is located at 75% chord from the leading edge, and the freestream Mach numbers are selected as 0.5, 0.825 and 0.85 to compare the present results with the experiment. To investigate the effect of the flap pulse amplitude β_1 in eqn (4), the GAF results are obtained for several values of β_1(0.01, 0.05, 0.10 and 0.50°). In this analysis, β_0 is set to be 0°. At $M_\infty = 0.5$ and 0.825, the steady shock wave does not occur on the airfoil surface. At $M_\infty = 0.85$ the steady shock wave occurs at about 50% chord station of the airfoil surface, not on the flap surface. Thus the flow conditions around the flap surface can be considered to be locally linear and the transient pulse method can be successfully applied. The GAF results for the different pulse amplitudes, which are not shown here, are coincident with one another and have little relations with the flap pulse amplitudes in these cases. Hereafter, all of the GAF results were calculated for 0.5° transient pulse amplitude.

Figure 6 shows comparison of the hinge moment between the present results by the transient pulse method and the experiment given in Ref. [16]. In Fig. 6a, the hinge moment coefficients are given when M_∞ is 0.5. The present results are in good agreement with the experiment and those of the thin airfoil theory, and those for the 6% thickness airfoil are very close to the experiment. Figure 6b and c show the hinge moment coefficients when M_∞ is 0.825 and 0.85, respectively. The present results are in better

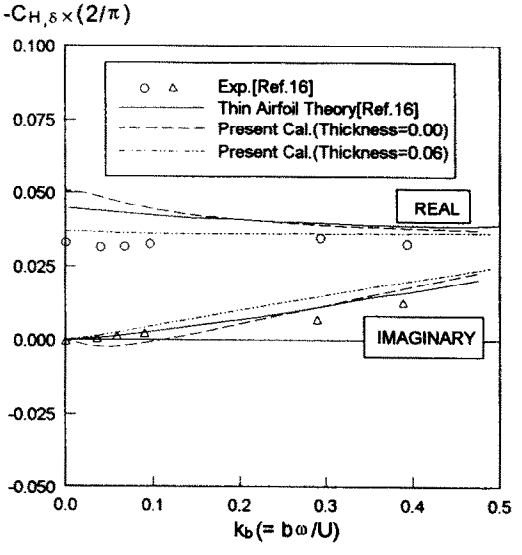

(a) M_∞=0.5

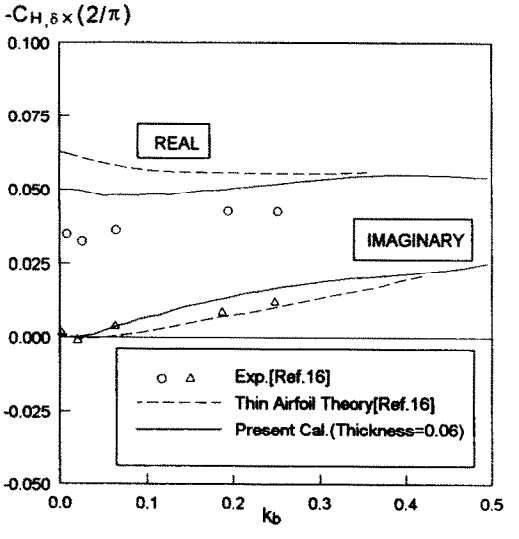

(b) M_∞= 0.825

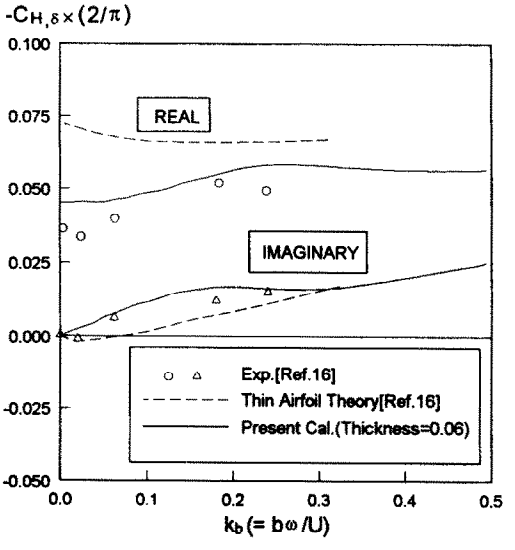

(c) M_∞= 0.85

Fig. 6. Generalized aerodynamic forces for the NACA64A006 airfoil with a trailing edge flap.

agreement with the experiment than those of the thin airfoil theory. From these results, it is concluded that the present method can be used for the calculation of GAFs.

Aeroelastic analysis

For the transonic aeroelastic analysis, both the U–g linear method and the time integration method are applied to an aeroelastic system with flap degree of freedom. The U–g method uses the Fourier transformation by which the pulse time data are transformed to the generalized aerodynamic forces in the frequency domain. Thus the linear assumption is introduced for the calculation of unsteady aerodynamic forces in the U–g method, whereas the time integration method, which solves the fluid and structural equation simultaneously, does not have any linear assumption. The aeroelastic parameters in eqns (5–7) are chosen as $r_\beta = 0.06$, $\mu = 52.1$, and $\omega_\alpha = 0.826$, whose data were used in Ref. [5]. The airfoil section used in this analysis is NACA64A006. The aeroelastic analyses are carried out for three points of view. First, the effect of structural damping coefficient on the flutter is investigated when Mach number is 0.91. Also, the effect of Mach number is studied when g_β is 0.0001 and the effect of the initial flap angle is investigated when $M_\infty = 0.85$ and $\beta_0 = 3.0$–$5.0°$.

Figure 7 shows the flutter boundaries for the NACA64A006 airfoil with a flap according to the frequency ratio ($\omega_\beta/\omega_\alpha$) at $M_\infty = 0.91$ when g_β are 0.0000, 0.0001 and 0.0003. When g_β is 0.0000, both the result calculated by the time response method and that by the U–g method are compared, and a slight difference is revealed between the two results. However, the U–g linear method predicts the flutter

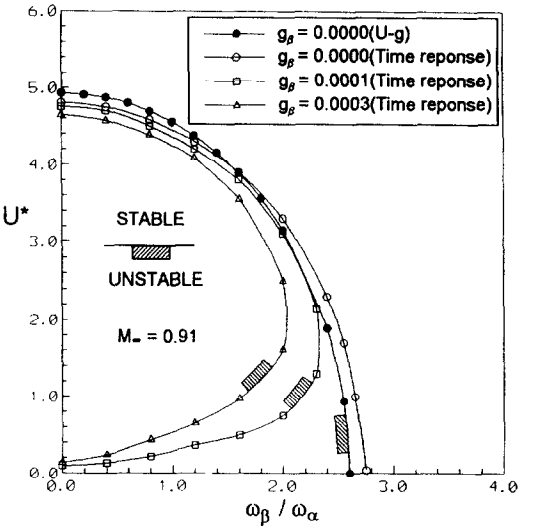

Fig. 7. The effect of structural damping coefficient g_β on the nondimensional flutter speed of an aeroelastic system with a flap ($M_\infty = 0.91$, $r_\beta = 0.06$, $\mu = 52.1$, $\omega_\alpha = 0.826$, $\beta_0 = 0.0°$).

boundaries reasonably well even though the shock is located on the flap surface ($M_\infty = 0.91$). As g_β increases, the lower flutter boundaries appear and the instability region becomes smaller. These flutter envelopes are similar to the bending–aileron and torsion–aileron flutter boundaries in 3 d.f. (plunge, pitch, and aileron) aeroelastic system in Ref. [6].

Figure 8 shows the time response result of the upper flutter boundary at $g_\beta = 0.0000$ and $\omega_\beta/\omega_\alpha = 1.60$ and that of the lower flutter boundary at $g_\beta = 0.0003$ and $\omega_\beta/\omega_\alpha = 1.60$ when Mach number is 0.91. In the present study, the initial conditions are $\beta(0) = 0.0$ and $d\beta(0)/dt = 0.01$.

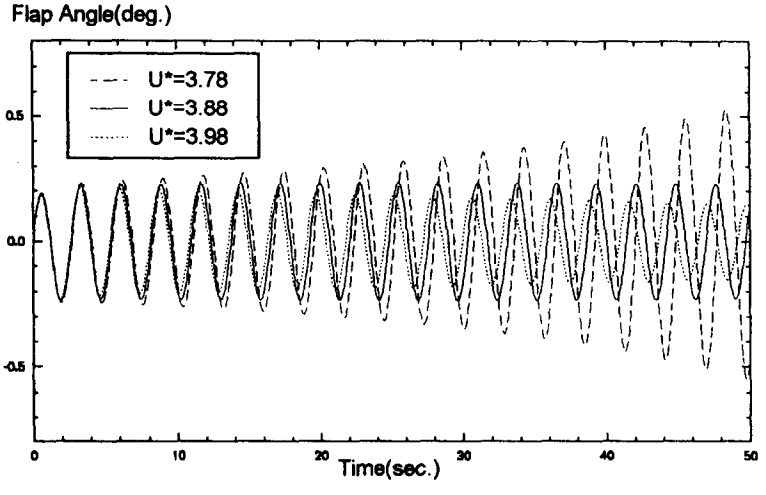

(a) g_β=0.0000, $\omega_\beta/\omega_\alpha$=1.60

Fig. 8. The typical time responses of an aeroelastic system with a flap (NACA64A006, $M_\infty = 0.91$, r_β-0.06, $\mu = 52.1$, $\omega_\alpha = 0.826$, $\beta_0 = 0.0°$). (*Continued opposite.*)

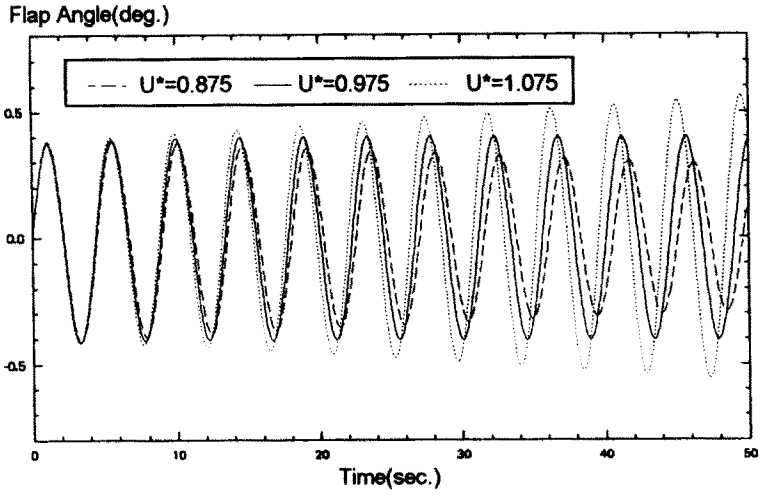

(b) g_β=0.0003, $\omega_\beta/\omega_\alpha$=1.60

Fig. 8—*Continued.*

The nondimensional flutter speed vs frequency ratio for various Mach numbers is given in Fig. 9. All data were obtained by the time integration method when g_β is 0.0001. As the Mach number increases, the instability region becomes larger. In the present case, the steady shock is located on the flap surface (not shown here) at $M_\infty = 0.89$–0.93 and moves to the trailing edge as the Mach number increases. Thus, the flap flutter occurs more easily when the shock is located on the flap surface and far from the flap hinge axis. As shown in Figs 7 and 9, the flutter region can be reduced by increasing the frequency ratio $(\omega_\beta/\omega_\alpha)$.

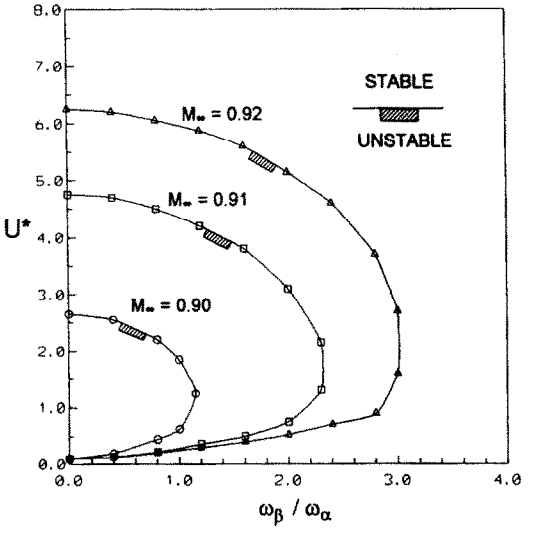

Fig. 9. The effect of Mach number on the nondimensional flutter speed of an aeroelastic system with a flap (NACA64A006, $r_\beta = 0.06$, $g_\beta = 0.0001$, $\mu = 52.1$, $\omega_\alpha = 0.826$, $\beta_0 = 0.0°$).

Figure 10 shows the effect of the initial flap angle ($\beta_0 = 3.0$–$5.0°$) on the flutter speeds and frequencies. When β_0 is 0, 0.5, 1.5, 2.0 and 2.5°, the flutter analyses were also carried out, but the critical neutral point did not occur. If β_0 is not zero in the present aeroelastic system, the airfoil and pressure distributions of upper and lower surfaces are not symmetric. Thus, the linear U–g results by the transient pulse method can be different according to positive (downward) or negative (upward) pulse inputs. The mean values of the U–g results by the positive ($\beta_1 = +0.5°$) and negative ($\beta_1 = -0.5°$) pulses are plotted in Fig. 10. The results between the U–g method and the time integration method have some differences. This difference become large as β_0 increases. This is because the linear assumption of the transient pulse method is improper when β_0 is large, even though the difference is small in this case when β_0 is 5°. The instability region is located below the critical flutter line because the structural damping is zero and becomes large as the initial flap angle increases.

CONCLUSIONS

In the present study, flutter analysis has been carried out for aeroelastic systems with a flap in a transonic flow regime. Aeroelastic results are obtained by solving Euler equations using a finite volume method and a fourth order Runge–Kutta time-stepping scheme.

For the verification of the present Euler code, the pressure distributions over the NACA64A010 airfoil are obtained at $M_\infty = 0.8$ when the initial flap angle increases from 0 to 6° with a 2° increment. The present numerical method provides quite accurate shock strength and shock locations for various initial

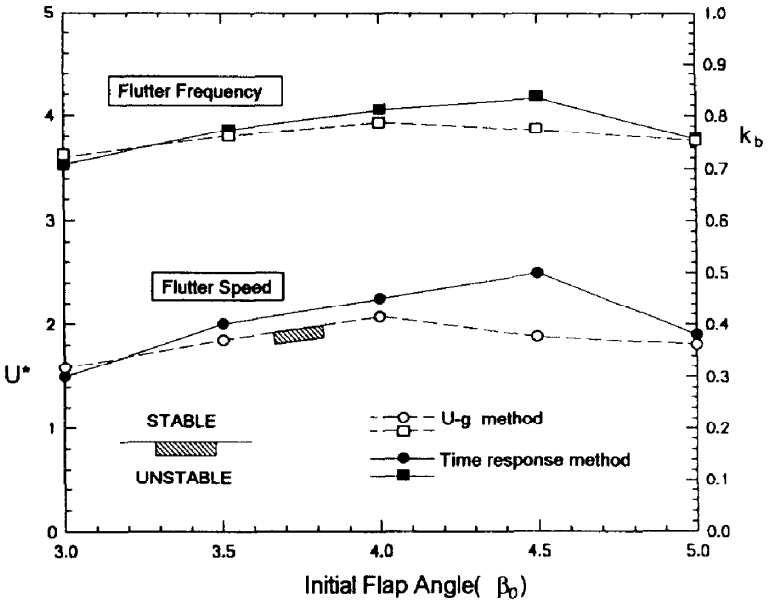

Fig. 10. The effect of initial flap angle on the nondimensional flutter speed of an aeroelastic system with a flap (NACA64A006, $M_\infty = 0.85$, $r_\beta = 0.06$, $g_\beta = 0.0$, $\mu = 52.1$, $\omega_\beta/\omega_\alpha = 1.5$, $\omega_\alpha = 0.826$).

flap angles, and unsteady pressure distributions are obtained in the time domain for the NACA64A006 airfoil with a flap. Also, generalized aerodynamic forces are calculated using the transient pulse method in the frequency domain. The present results by Euler code are in a good agreement with the experiment in subsonic and transonic speeds.

Flutter results are obtained for the NACA64A006 airfoil with a flap using both the U–g and the time integration method. When Mach number is 0.91, the region of the flutter boundary becomes smaller as the structural damping increases. Also, the flutter region increases as the Mach number increases. The effect of initial flap angle are also investigated and the instability region increases as the initial flap angle increases when the initial flap angle is less than 4°.

Some discrepancies are observed between the results by the U–g linear method and time response analysis since the linear assumption for the impulse method is improper when the initial flap angle becomes large or the steady shock is located on the flap surface. However, the U–g method still gives reasonable results compared with those of the time integration method.

REFERENCES

1. J. W. Edwards and J. B. Malone, Current status of computational methods for transonic unsteady aerodynamics and aeroelastic applications. NASA TM 104191 (1991).
2. J. G. Leishman, Unsteady lift of a flapped airfoil by indicial concepts. *J. Aircr.* **31**, 288–297 (1994).
3. R. Magnus and H. Yoshihara, The transonic oscillating flap. paper-76-327, In: *AIAA 9th Fluid and Plasma Dynamics Conf.*, San Diego, CA, 14–16 July, (1976).
4. W. F. Ballhaus and P. M. Goorjian, Implicit finite-difference computations of unsteady transonic flows about airfoils. *AIAA J.* **15**, 1728–1735 (1977).
5. T. Y. Yang and J. T. Batina, Transonic time-response analysis of three degrees of freedom conventional and supercritical airfoils. AIAA paper-82-0688, pp. 256–266 In: *AIAA/ASME/ASCE/AHS 23rd Structures, Structural Dynamics and Materials Conf.*, New Orleans, LA, May, (1982).
6. T. Y. Yang and C. H. Chen, Transonic flutter and response analyses of two three-degree of freedom airfoils. *J. Aircr.* **19**, 875–888 (1982).
7. J. L. Steger and H. E. Bailey, Calculation of transonic aileron buzz. *AIAA J.* **18**, 249–255 (1980).
8. W. J. Chyu and L. B. Schiff, Nonlinear aerodynamic modeling of flap oscillations in transonic flow: a numerical validation. *AIAA J.* **21**, 106–113 (1983).
9. W. Schmidt and A. Jameson, Euler solvers as an analysis tool for aircraft aerodynamics, In: *Advances in Computational Transonics (Recent Advances in Numerical Methods and Fluids)* (Edited by W. G. Habashi), Vol. 4, pp. 371–404. Pineridge Press, Swansea (1985).
10. C. A. J. Fletcher, Computational Techniques for fluid dynamics 2. In: *Computational Physics*, 2nd edn, pp. 81–127. Springer, Berlin (1991).
11. J. L. Stager and R. L. Sorenson, Note: automatic mesh-point clustering near a boundary in grid generation with elliptic partial differential equations. *J. Comput. Phys.* **33**, 405–410 (1979).
12. R. D. Raush, J. T. Batina and H. T. Y. Yang, Euler flutter analysis of airfoils using unstructured dynamic meshes. *J. Aircr.* **27**, 436–443 (1990).
13. B. A. Robinson, J. T. Batina and H. T. Y. Yang, Aeroelastic analysis of wings using the Euler equations with a deforming mesh. AIAA paper-90-1032-CP, pp. 1510–1518 (1990).
14. S. R. Bland and J. W. Edwards, Airfoil shapes and thickness effects on transonic airloads and flutter. *J. Aircr.* **21**, 209–217 (1984).
15. S. S. Davis, Data set 2-NACA64A010 (NASA Ames Model) oscillating pitching, compendium of unsteady aerodynamic measurements, AGARD-R-702, pp. 2–22 (1982).
16. H. Tijdeman, Investigations of the transonic flow around oscillating airfoils. National Aerospace Laboratory, The Netherlands, NLR-TR-77090U, pp. 60–62 (1977).